GENERAL PHYSICS

I. MOLECULAR BEAMS*

Academic and Research Staff

Prof. J. R. Zacharias
Prof. J. G. King
Prof. J. R. Clow
Dr. T. R. Brown
Dr. E. H. Jacobsen
Dr. M. G. R. Thomson
Dr. J. C. Weaver
F. J. O'Brien

Graduate Students

S. A. Cohen
W. B. Davis
H. F. Dylla
G. A. Herzlinger
D. G. Payan
D. M. Payne

A. EVAPORATION OF NEUTRAL ATOMS FROM He II STIMULATED BY HEAT PULSES

1. Introduction

Since the first measurements of the velocity distribution of atoms evaporating from the surface of bulk liquid helium by Johnston and King,[1] several theories have been advanced to explain the helium evaporation process.[2] In these theories, the excitations in liquid He II, phonons and rotons, play an important role in the evaporation mechanism.

In this report, we discuss an experiment designed to study the evaporation mechanism and describe an apparatus built to carry out this experiment.

In the Johnston-King evaporation experiment the velocity distribution of the evaporation of atoms from bulk liquid helium was measured and they found that the distribution was a Maxwell-Boltzmann distribution characterized by an effective temperature approximately 1°K hotter than the source. Attempts to explain this unusual result centered on the part that phonons and rotons play in the conversion of internal energy of the bulk helium into free particles in the vapor. Phonon conversion at the surface would give a broad low-energy spectrum of particles in the vapor, while roton conversion would give a high-energy tail starting at $\Delta - \mu = 1.5°K$, where Δ is the roton minimum equal to 8.68°K, and μ is the latent heat of evaporation equal to 7.18°K per atom. This combination of conversion processes could explain the higher energy velocity distribution of the vapor.

When McWane[3] and Tinker[4] repeated the experiment under better experimental conditions, however, they found that the temperature shift in the vapor was not greater than 0.3°K, and in all probability that the temperature of the evaporating atoms was in equilibrium with the bulk fluid. This shows that we still do not understand the processes that are important in the creation of evaporation atoms from the surface of

*This work was supported by the Joint Services Electronics Programs (U.S. Army, U.S. Navy, and U.S. Air Force) under Contract DA 28-043-AMC-02536(E).

the bulk fluid and, in particular, how rotons and phonons interact with the surface and how energy is transported across the surface.

One way of investigating the surface interactions of phonons and rotons is to direct a beam of these excitations at the surface. These beams of phonons and rotons are the well-known phenomena of second sound in liquid He II.[5] It was demonstrated early in the investigation of second sound, that second-sound pulses incident on the surface of the bulk liquid could be detected by the density variation in the vapor.[6] The density variations in the vapor are due to the heating of the surface and the resultant evaporation of atoms when the pulse of second sound arrives at the surface. This suggests that by applying neutral-beam techniques, the interactions of phonons and rotons at the surface of liquid He II could be studied.

2. Experimental Apparatus

The study of liquid helium by neutral-beam techniques in the temperature range of interest has presented many experimental problems. Various methods[3,7] have been developed in this laboratory to deal with them and apparatus utilizing these methods has been built.

The apparatus (see Fig. I-1) comprises a stainless-steel vacuum chamber, a He^3-He^4 pot structure isolated from the He^4 bath by a stainless-steel pumping tube, a copper septem, a field-ionizing needle, and an electron multiplier. The whole can is immersed in a standard He^4 dewar containing a liquid-helium bath which can be pumped down to 1.2°K. By the use of standard one-shot He^3 refrigeration methods, a no-load temperature of 0.3°K can be obtained on the He^3-He^4 pot structure.

The He^3-He^4 pot structure (see Fig. I-2) is crucial to the experiment. This structure is composed of the He^3 pot with sintered copper bottom, an He^4 fill line and sintered heat exchanger, and an oven onto which the He^4 pot is soldered. The He^4 pot is a stainless-steel tube, of 0.125 in. diameter, with an epoxy bottom through which a copper wire has been embedded. The heater is a carbon resistor built up from an aquadag solution deposited on the epoxy bottom. A voltage is placed across the heater to the grounded walls by the central copper-wire lead.

The He^4 pot is filled by letting in a predetermined amount of gas from a gas-handling system at room temperature into the He^4 fill line. This line passes down through a sintered copper heat exchanger in the He^4 bath, into a thin wall capillary passing down the He^3 pump line into the sintered copper heat exchanger in the He^3 pot. The liquid He^4 is then allowed to fall into the He^4 pot from the end of a capillary of small diameter.

This design for the unusual He^4 fill system where the liquid drops into the He^4

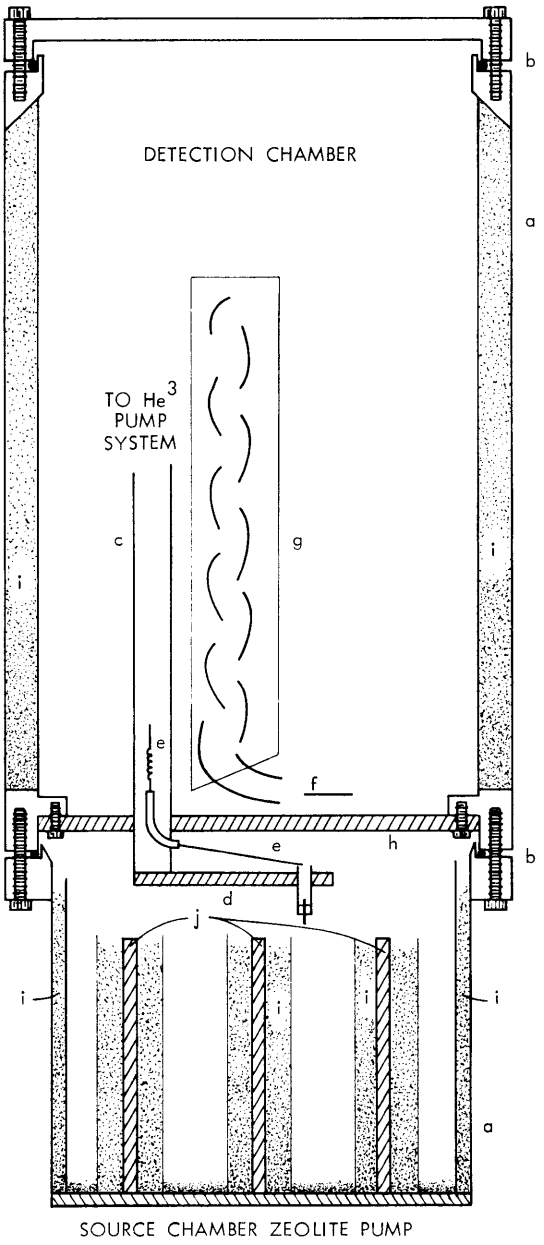

(a) STAINLESS-STEEL CHAMBER
(b) LEAD O-RING SEAL
(c) He^3 PUMP LINE
(d) He^3-He^4 POT STRUCTURE
(e) He^4 FILL LINE
(f) FIELD IONIZING NEEDLE
(g) ELECTRON MULTIPLIER
(h) COPPER SEPTUM
(i) ZEOLITE
(j) COPPER RODS AT BATH TEMPERATURE

Fig. I-1. Apparatus for studying the evaporation of helium atoms from He II stimulated by heat pulses.

pot is required because of the superfluid qualities of He^4 liquid. If the He^4 pot on the He^3 refrigerator were directly connected to the bath through a fill capillary, then there would be a large heat leak to the He^3 refrigerator, which would limit the lowest temperature that could be achieved. In McWane's experiment,[3] he was unable to achieve a temperature lower than 0.5°K, because of the 5-MW heat leak from the bath. Thus, by decoupling the He^4 pot from the bath, we eliminate this large heat leak and should be able to obtain temperatures down to 0.3°K. We could have obtained the same decoupling effect by changing the size and length of the fill capillary,[8] but if the fill capillary is made too small in cross section, then the He^4 pot could not be filled, on account of film flow out of the pot.

The fact that liquid He II forms films and that these films can flow and transport bulk helium is well known.[4] The rate of film flow from the pot is proportional

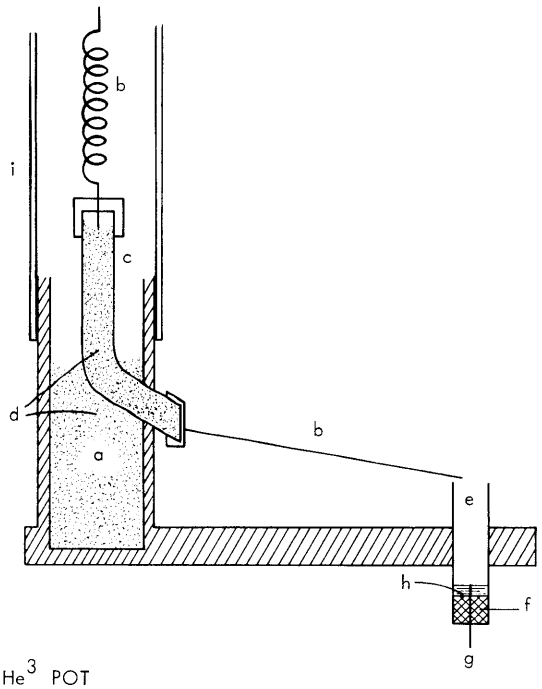

(a) He^3 POT
(b) He^4 FILL LINE
(c) He^4 HEAT EXCHANGER
(d) SINTERED COPPER
(e) He^4 POT
(f) EPOXY BOTTOM
(g) HEATER LEAD
(h) AQUADAG HEATER
(i) He^3 PUMP LINE

Fig. I-2. He^3-He^4 pot structure.

to the perimeter of the pot, and for a pot of 1/8 in. diameter, is of the order of 10^{18} atoms/second. The rate of evaporation is proportional to the surface area, and at 0.5°K is approximately 10^{17} atoms/second. The rate of evaporation from the pot surface and those surfaces covered by the films are the same, but since the film covers larger areas, the pumping system must be designed for the flow rates of the films.

Pumping is done entirely by Molecular Seive (zeolite) in the form of pellets. In order that the zeolite pump properly, it must be in good thermal contact with the He^4 bath, as the latent heat of adsorption of the helium gas will quickly heat up the zeolite and reduce its effectiveness.

The vacuum chamber is divided into two pumping regions by the copper septem, the detector chamber, and the lower source chamber. In the upper chamber the zeolite is held against the walls of the chamber by thin mesh screening.

The lower chamber is a specially designed zeolite pump (see Fig. I-1). The zeolite is held in 29 cold fingers projecting from the bottom of the chamber and on the walls by thin mesh screening. The core of each finger is a copper rod in direct contact with the He^4 bath. The rate at which zeolite pumps is a function of its temperature and surface area. Thus the design maximizes the surface area of the zeolite and the thermal contact with the He^4 bath.

The beam from the He^4 pot passes through a small exit slit in the septum, and is detected by means of field ionization at the tip of a sharp tungsten needle maintained at 10-15 kV. The ions are detected by an Allen type of electron multiplier having a gain of $\sim 10^6$. The resultant pulses are then amplified and counted by standard pulse amplification and counting systems.

3. Preliminary Tests

Tests have been made at liquid-helium temperatures to test the various components. The results, at present, are very sketchy but encouraging.

After a 12-16 hour cool-down at liquid-helium temperatures the count rate for a 600 Å needle at 10 kV was 1 or 2 counts/second, corresponding to a pressure in the 10^{-13}-10^{-12} Torr range. By letting gas in the helium fill line at low flow rates, we were able to see a beam of atoms from the source chamber. We have not yet been able to determine the pumping speed of the zeolite pumping, but hope to do so soon. Also, because of various malfunctions, we have not determined with certainty that we have collected liquid in the He^4 pot. Indications are, however, that we shall be able to fill the pot and achieve temperatures in the range 0.35-0.4°K at the low end.

W. B. Davis

References

1. W. D. Johnston, Jr. and J. G. King, Phys. Rev. Letters 16, 1191 (1966).
2. For a review and references see J. W. McWane and R. F. Tinker, Quarterly Progress Report No. 96, Research Laboratory of Electronics, M. I. T., January 15, 1970, pp. 2-11.
3. J. W. McWane, Ph. D. Thesis, M. I. T., 1970 (unpublished).
4. R. F. Tinker, Ph. D. Thesis, M. I. T., 1970 (unpublished).
5. J. Wilks, Properties of Liquid and Solid Helium (Clarendon Press, Oxford, 1967).
6. C. T. Lane, H. A. Fairbank, and W. M. Fairbank, Phys. Rev. 71, 600 (1947).
7. W. D. Johnston, Jr., Ph. D. Thesis, M. I. T., 1966 (unpublished).
8. B. Beetman and T. A. Kitchens, Cryogenics 8, 36 (1968).

B. CORRECTION OF THE SPHERICAL ABERRATION OF ELECTRON MICROSCOPE OBJECTIVE LENSES USING TRANSPARENT FOILS

1. Introduction

Early in the history of the development of the electron microscope it was found by Scherzer[1] that any conventional electron lens would have a coefficient of spherical aberration that is positive and nonzero. By a conventional lens we mean a static electric or magnetic field possessing cylindrical symmetry about the electron beam axis, with no free charges or electric currents within the space traversed by the beam. The aberration is always found to be such that marginal rays are focussed more strongly than paraxial ones (Fig. I-3).

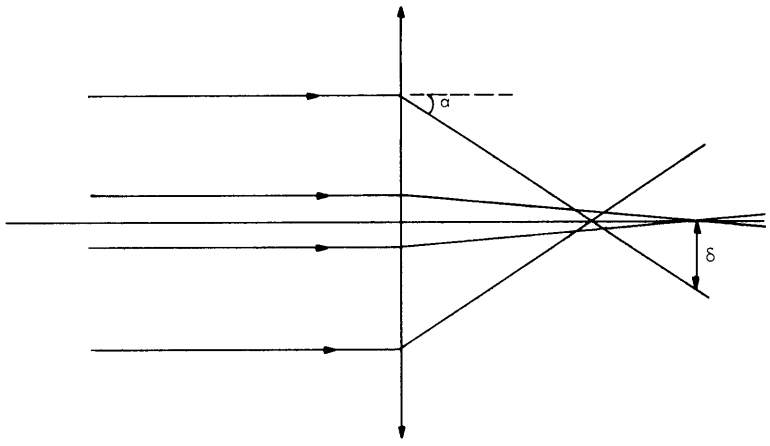

Fig. I-3. Cylindrically symmetric lens with positive spherical aberration coefficient.

The ill effects of spherical aberration, and at the same time of chromatic aberration, can be minimized by reducing the focal length of the lens, and by using a magnetic, rather than an electrostatic, field. The focal length is limited by the maximum attainable magnetic field strengths and the mechanical difficulties involved in constructing the lens pole pieces. In commercial high-resolution instruments it will be less than 1 cm, and in at least one research microscope it is less than 1 mm with a 30-keV electron beam. The best achieved point-to-point resolution is around 2 Å. The construction of these lenses has been brought to a fine art, involving tolerances of ~1 μm in critical areas, and further development along these lines is expected to be very slow. (The reader is referred to any electron optics textbook, for example, Klemperer.[2])

An obvious alternative approach is to construct suitably "unconventional" lenses in which at least one of the assumptions made in Scherzer's theorem becomes invalid. Most of the work has been directed toward the removal of cylindrical symmetry and its replacement with two mutually perpendicular planes of symmetry. Such lenses are called "doubly symmetric" or "strong focussing," and include quadrupoles and octopoles (Fig. I-4).[3] Unfortunately, a large number of lens elements are required even to

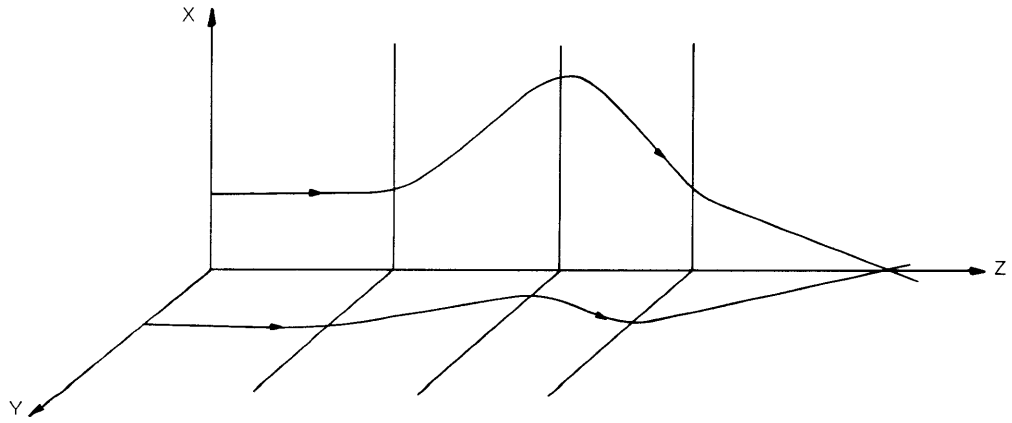

Fig. I-4. "Doubly symmetric" triplet, employing 3 quadrupole lenses. The behavior in the X-Z and Y-Z planes differs, but a stigmatic image may still be formed.

produce a composite that will correct the aberration of a round lens; typically, four quadrupoles and three octopoles will be used. To improve upon the best resolution achieved thus far, tolerances of the order of 1 μm are required, but now they apply to the positioning of 40 pole pieces instead of just the machining tolerances of two circular ones. It is not surprising that such a lens has never been successfully made.

A second method is to vary the excitation of an electrostatic lens while the electrons are passing through. Unfortunately, the transit time is very short at the

energies which are useful in electron microscopy, so the design involves the use of alternating voltages of kilovolt magnitude and 10^9 Hz frequency. Furthermore, the electron beam must be chopped into pulses 10^{-12} s long.

The technique with which we are primarily concerned is the introduction of electrostatic charges within the beam. In other work this has been attempted by the introduction of space charge, but it has been found very difficult to control and stabilize the large charge densities that are required. Because of the lack of success of the high-frequency and space-charge experiments, there is very little published work.

The distribution of charge can be well defined by introducing conductors within the electron beam. This conductor can be either a fine mesh, or a very thin metal foil. The former suffers from the irregularity of the distribution across the mesh holes, while the latter usually involves foils of such thickness that the beam is badly scattered.[4,5]

2. Foil Lenses

In a foil lens we place one or more very thin metal foils across the axis. The cylindrical symmetry of the system is preserved; the beam passes perpendicularly through the foil (Fig. I-5). By shaping the foils and introducing nearby charged electrodes we can obtain a useful distribution of charge on the foil surface, and hence can control the focussing properties and the aberrations of this lens. In the following discussion we speak of the axial potential distribution through the lens, rather than of the charge density, since the former is physically more significant.

The difficulties lie in the construction of acceptable foils. These must accurately

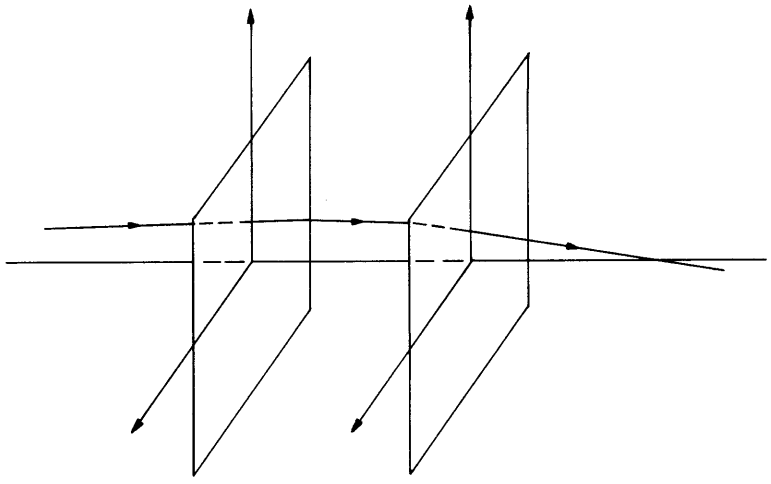

Fig. I-5. A foil lens is constructed by placing one or more thin conducting foils at right angles to the axis. Other electrodes produce the required charge and potential distribution.

hold their shape over an area a fraction of a millimeter square, and yet be sufficiently thin that a negligible fraction of the beam is scattered. They will also be subjected to large electrostatic fields. Theoretical scattering results evaluated at 65 keV indicate that if we can make a 100 Å thick beryllium foil, then this will scatter 5% of the beam elastically and 30% inelastically.[6] We feel that these amounts, which at first sight seem large, will not be prohibitively so. The inelastically scattered electrons, having lost at least a few eV energy, can be removed with a spectrometer and, by suitable placing of apertures, it should be possible to remove most of the elastically scattered electrons. Thus there will be a reduction in intensity, but only a small degradation in image quality. Experiments on the construction of these foils are being performed by E. H. Jacobsen.

By applying Laplace's equation, $\nabla^2 V = 0$, we can determine the potential at all off-axis points from knowledge of the potential and its Z-derivations on the axis; that is, from $V(0,Z)$ we can find $V(r,Z)$. Thus the electron-optical properties of these foil lenses can be visualized most easily in terms of the axial potential. To a first approximation, the focal length F of a lens is given by

$$\frac{1}{F} = \int_{\text{Object}}^{\text{Image}} (V''/4V)\, dZ$$

where the prime denotes $\partial/\partial Z$, and V is measured relative to the potential at which the electrons would be at rest.

A strongly convergent lens will thus have a net positive curvature of the potential (V"), and similarly we can obtain a strongly divergent lens by specifying a net negative curvature. (Without foils we would be unable to do the last.)

The third-order spherical aberration can less accurately be considered a function of

$$\frac{1}{\sqrt{V_o}} \int_{\text{Object}}^{\text{Image}} (V^{iv}/\sqrt{V})\, dZ,$$

where V_o is the potential in the plane in which the aberration is measured, or to a slightly better approximation as a function of

$$\frac{1}{\sqrt{V_o}} \int_{\text{Object}}^{\text{Image}} (V^{iv}/\sqrt{V} - V''^2/V^{3/2})\, dZ.$$

The most promising use of the lens is in conjunction with a magnetic objective lens, arranging for the spherical aberrations to cancel each other. The two lenses may

be placed next to each other, or the foils may be constructed within the bore of the magnetic lens. The last arrangement has advantages that we shall not discuss here. To achieve an over-all aberration of zero, we require $\int (V^{iv}/\sqrt{V})\, dZ$ to be as large as possible. Figure I-6 shows examples of suitable axial potential distributions using fairly simple electrodes and flat foils. Figure I-6a shows a one-foil converging lens, and Fig. I-6b a two-foil diverging lens.

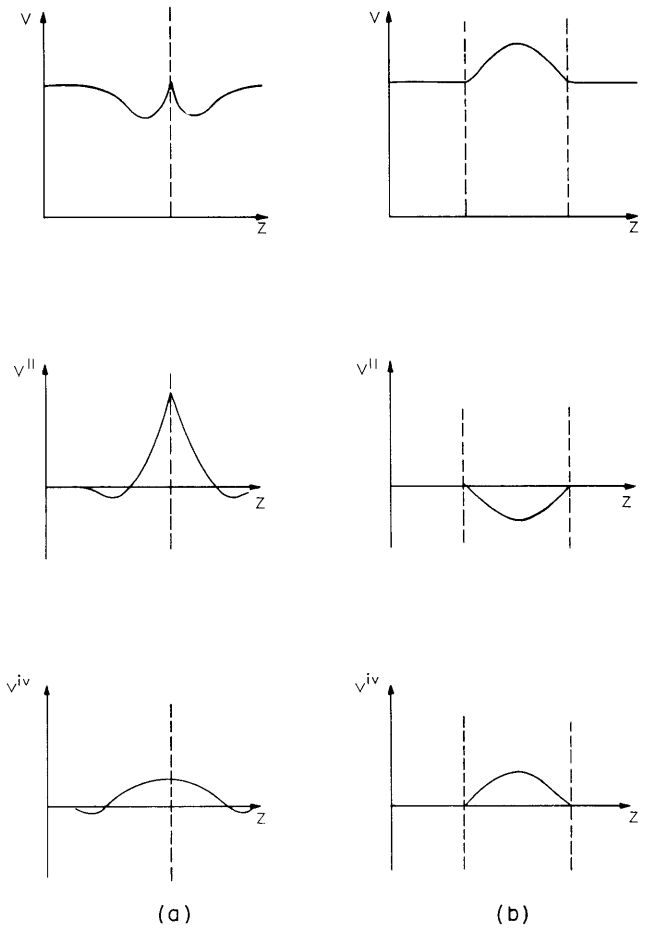

Fig. I-6. Examples of potential distributions in foil lenses. Both correct spherical aberration. (a) one-foil converging lens; (b) two-foil diverging lens.

These suggestions have been accurately evaluated by extensive numerical integration, using a development of the aberration formulation of Hawkes,[7] and the ideas mentioned above have been confirmed. In particular, using the configuration in Fig. I-6b, with a foil separation of approximately 1 cm, we can correct the spherical aberration of a magnetic lens with ~1 cm focal length. The potential variation

within the lens is 10% of the external beam voltage.

3. Conclusion

It is apparently simple to design a one- or two-foil electrostatic lens that will correct the aberrations of a magnetic objective lens. The difficulties lie in construction of suitably thin, strong foils, and there will inevitably be some degradation of the image quality caused by the elastic and inelastic scattering of the electron beam.

It also appears possible that we may be able to extend the design to include simultaneous correction of the paraxial chromatic aberration, but the results, at present, are speculative.

M. G. R. Thomson

References

1. O. Scherzer, Z. Physik 101, 593 (1936).
2. O. Klemperer and M. E. Barnett, Electron Optics (Cambridge University Press, London, 1971).
3. P. W. Hawkes, "Quadrupoles in Electron Lens Design," Advances in Electronics and Electron Physics Supplement 7 (Academic Press, New York, 1970).
4. J. L. Verster, Philips Research Reports 18, 465 (1963).
5. J. E. Barth, Ph. D. Thesis, University of Arizona, 1967.
6. F. Lenz, Z. Naturforsch. 9a, 185 (1954).
7. P. W. Hawkes, "Quadrupole Optics," Springer Tracts in Modern Physics Vol. 42 (Springer-Verlag, Berlin, 1966).

C. AN ACOUSTIC MEANS OF DETECTING AN ELECTRON-PROTON CHARGE DIFFERENCE

This report describes a new experimental technique for testing the electrical neutrality of molecules. The assumed equality of the electron and proton charges represents a symmetry in nature which corresponds to no known conservation law, but is based directly on a series of sensitive experimental measurements dating from 1925 (see Table I-1). These measurements have involved three different experimental techniques: the gas-efflux method, the isolated-body method, and the molecular-beam method. The first two methods involve the measurement of the total charge on a macroscopic number of molecules, and the third method involves the measurement of the deflection of the trajectory of a beam of molecules in a region of homogeneous electric field. When care has been taken to eliminate the effect of ions and other charged particles (as in methods 1 or 2), the findings of these experiments are consistent with the assumption that matter is neutral; that is, the measured charge per molecule is

Table I-1. Comparison of neutrality measurements.

	Method	Molecule	Upper Limit for $\|Q\|$	Upper Limit for ϵ	Reference
Millikan	(2)	–	–	1×10^{-16}	1
Hopper and Laby	(2)	–	–	5×10^{-17}	2
Stover, Moran and Trischka	(2)	–	–	1×10^{-19}	3
Piccard and Kessler	(1)	CO_2	2×10^{-19}	4×10^{-21}	4
Hillas and Cranshaw	(1)	A	8×10^{-20}	2×10^{-21}	5
		N_2	12×10^{-20}	5×10^{-21}	
King	(1)	H_2	2×10^{-20}	1×10^{-20}	6, 7
		He	4×10^{-20}	1×10^{-20}	
		SF_6	7×10^{-21}	5×10^{-23}	
Hughes	(3)	CsI	4×10^{-20}	2×10^{-15}	8
Zorn, Chamberlain, and Hughes	(3)	Cs	1×10^{-17}	5×10^{-19}	9
		K	4×10^{-17}	1×10^{-18}	
		H_2	2×10^{-15}	1×10^{-15}	
		D_2	3×10^{-15}	1×10^{-15}	
Fraser, Carlson, and Hughes	(3)	Cs	2×10^{-18}	1×10^{-20}	10
		K	1×10^{-18}	3×10^{-20}	
Shapiro and Estulin	(3)	n	6×10^{-12}	6×10^{-12}	11
Shull, Billman, and Wedgwood	(3)	n	2×10^{-18}	2×10^{-18}	12

zero within the experimental errors.

This upper limit for the molecular charge can then be used to establish upper limits on an electron-proton charge difference, ϵe ($\epsilon \ll 1$, $e = 4.8 \times 10^{-10}$ esu) and the neutron charge, q_n. With the condition that $\epsilon e = q_n$ which follows from the assumption of charge conservation in the beta decay of the neutron ($n \rightarrow p + e^- + \bar{\nu}$) with the additional assumption of zero charge carried by the antineutrino, the upper limit for the electron-proton charge difference is the measured molecular charge divided by the total number of nucleons, $M = Z + N$.

The experiment described in this report presents an experimental method which is independent of the three existing methods just described. The sensitivity of the experiment has equaled the best published number for the upper limit of an electron-proton charge difference, (1×10^{-21} e), but more important, this limit does not represent the ultimate sensitivity of experiment. Also, this method is far less sensitive to the presence of ions and other free charged particles which necessarily complicate the interpretation of previous microscopic neutrality measurements.

The experiment concerns the effect of an oscillating electric field on a gas contained within a high-Q acoustic cavity. Under the assumption that the gas has a charge density because of a small charge, $M\epsilon e$, on each molecule, and a molecular polarizability, α, then the force per unit volume of the gas in the presence of the field is given by

$$F_v = nM\epsilon eE + \frac{n}{8\pi}\alpha\nabla E^2. \tag{1}$$

If the applied electric field is harmonically time-variant at the frequency ω_o, then the volume force will have an oscillating component at ω_o attributable to the first term and a component at $2\omega_o$, because of the second term. Such time-variant volume forces will give rise to harmonic pressure variations or sound waves in the gas. Mathematically, the divergence of the volume force is the source term for the wave equation for first-order pressure variations:

$$\nabla^2 p - \frac{1}{c^2}\frac{d^2 p}{dt^2} = \text{div } F_v. \tag{2}$$

The basis of an experiment to define an upper limit for the charge of a molecule is now apparent. The apparatus is designed to detect the presence of sound waves in the gas at the same frequency as the applied electric field: (i) if the medium is free of ions, (ii) if care has been taken to prevent coupling between the electrical and acoustic circuits, and (iii) if harmonic distortion in the electric field has been appropriately minimized to prevent coupling of the polarization signal at $2\omega_o$, then the detected sound wave at ω_o should be proportional to the charge on the molecule. Of

course, a null result is expected. Therefore the sensitivity of the experiment is limited by the ability to minimize the inherent noise sources (Johnson noise, background acoustics, and so forth) and the effective elimination of the experimental problems mentioned above. The experiment gains sensitivity by adjusting the frequency of the applied electric field to coincide with a cavity resonance, and by discriminating against all but this single frequency in the detection circuitry. Detection of the polarization signal at $2\omega_o$ offers a convenient means of calibrating the apparatus.

The acoustic cavity chosen for the experiment was a sphere, of 20-cm radius, constructed from two hemispheres, 1.5 mm thick. The cavity exhibited Q's greater than 10^3 for 1 atm of gas when excited in its first radial mode, thereby eliminating viscous boundary losses. The Q measurements were made with two different gases, N_2 and SF_6. The measurements with N_2 were useful because its acoustic properties are similar to air, and the microphone response was known for air. The actual neutrality measurements were made with SF_6 because of its large mass number (M = 146). Details of the spherical cavity are shown in Fig. I-7. In addition to two microphones and a

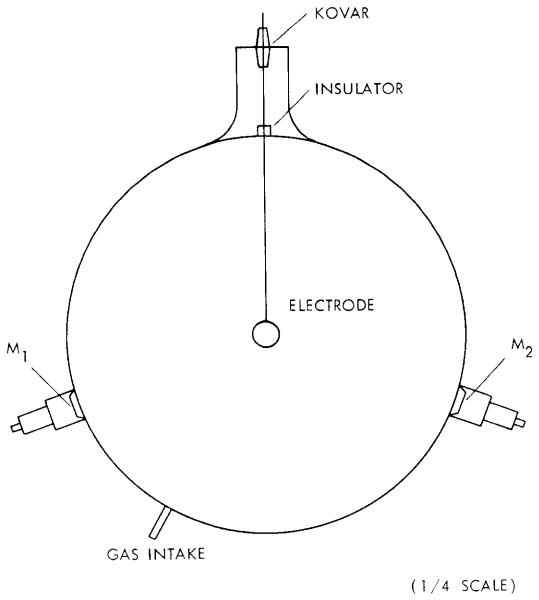

Fig. I-7. Spherical cavity.

gas intake on the periphery of the cavity, a high-voltage electrode, which is a 1 in. brass sphere, is supported at the center of the cavity. The cavity is mounted on an elastic support within a large iron vacuum chamber, which could be evacuated with a mechanical forepump as a means of acoustic isolation. All electrical and gas connections to the sphere are made flexible to prevent coupling of external vibrations.

The detection circuit begins with the microphones and ends with an analog signal on

a strip chart recorder proportional to the pressure differential at the microphone diaphragm. The microphones are so wired in series that acoustic signals add and electrostatic and magnetic pickup from the high-voltage electrode cancel. The resulting signal is first preamplified wideband and then amplified by a lock-in amplifier with a 0.1 Hz bandwidth referenced to the frequency of the high-voltage driving circuit. The cancellation of the pickup from the high-voltage circuit is not exact, because of asymmetries in the circuit parameters. A balance circuit provides an equivalent amount of signal of the same frequency but opposite phase to cancel the residual pickup at the input of the lock-in amplifier. Pickup can be distinguished from any true acoustic signal by its lack of frequency dependence in the vicinity of the acoustic resonance.

The largest source of inherent electrical noise is the Johnson noise of the resistive elements of the microphone windings. Figure I-8a shows the output of the detection circuit with a 600 Ω resistor replacing the microphones. The measured mean voltage deviation of $\delta V \approx 1.5 \times 10^{-9}$ V referred to the input agrees with the calculated value of the Johnson noise of a 600 Ω source. Figure I-8b shows the output of the

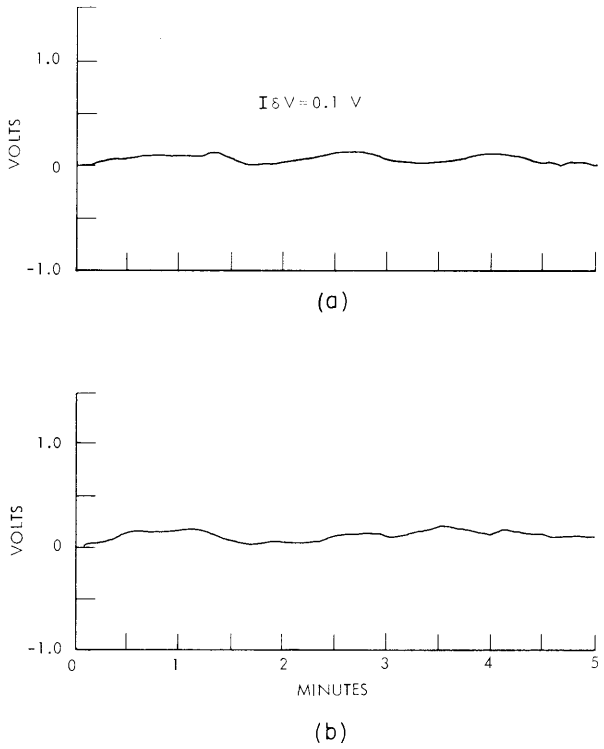

Fig. I-8. (a) Total electronic noise with 600 Ω resistor in place of microphones: $\delta V \approx 1.5 \cdot 10^{-9}$ V referred to input (f = 494 Hz, Δf = 0.1 Hz).
(b) Total noise with 12 psi SF_6 in cavity (f = 494 Hz, Δf = 0.1 Hz).

detection circuit with a pressure of 12 psi SF_6 in the cavity. Comparison of the two plots shows that the acoustic isolation of the cavity has attenuated the background acoustic noise to a level below that of the Johnson noise.

The high-voltage driving signal is provided by a transformer. The input of the transformer is the amplified output of the reference audio oscillator. Considerations in the design of this circuit included the prevention of any DC or second-harmonic components in the output signal which would couple a fraction of the real sound signals at $2\omega_o$ to the fundamental and mask the hypothetical charge signal. A 300-V battery in the high-voltage circuit provides a means of intentionally producing a signal at the fundamental frequency for the purpose of tuning the detection circuit. The DC voltage also sweeps the cavity of ions and charged particles that might interfere with the neutrality measurement.

The apparatus is calibrated at its resonant frequency ω_o by driving the high-voltage circuit at $\omega_o/2$, thereby producing a signal at ω_o, because of the polarizability of the molecules. (Sound is also produced at twice the fundamental, since the electric field exerts mechanical forces on the electrode structure, but this signal was calculated to be three orders of magnitude smaller than the polarization signal.) The measured polarization signal voltage $\Delta V_{SIG}/V^2$ divided by the calculated value of the polarization signal pressure $\Delta P_D/V^2$ yields the desired calibration, $\partial V_{SIG}/\partial P_D$. The calculation of P_D/V^2 involves solving the wave equation with the second term of Eq. 1 as the source term. The calculated value of the polarization signal pressure for 12 psi of SF_6 at 300°K is

$$\frac{P_D}{V^2} = 2.8 \times 10^{-5} \text{ dyne-cm}^{-2}/(\text{esu})^2. \tag{3}$$

Figure I-9 shows two measurements of the polarization signal with these same experimental conditions. The differences in the slopes of the two runs can be accounted for by temperature drifts within the cavity. By using the average slope V_{SIG}/V^2, the following number is obtained for the calibration

$$\frac{\partial V_{SIG}}{\partial P_D} = \frac{V_{SIG}}{V^2} \cdot \frac{V^2}{P_D} = 1.9 \times 10^2 \text{ V/dyne-cm}^{-2} \cdot \tag{4}$$

The calculation and measurement of the polarization signal was repeated for N_2. Since the microphone calibration in air (air = 0.78% N_2) is known, the calculated value of P_D/V^2 for N_2 can be multiplied by the response and the measured detection circuit gain. This predicted value of the N_2 polarization signal can be compared with the observed value as a check on the polarization calculation. The two values were found to agree by better than a factor of two, which is more than sufficient agreement

for its intended purpose.

The specific measurement of the neutrality of the SF_6 molecule now remains to

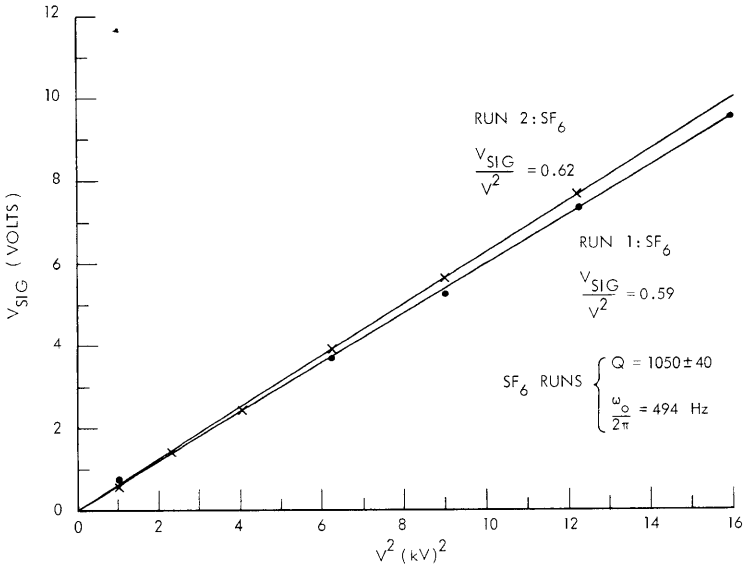

Fig. I-9. Polarization data.

be discussed. First of all, the wave equation was solved with a source term given by the product of the charge density $\rho = nM\epsilon e$ and the field within the cavity. The result, when solved for $M\epsilon$ is

$$M\epsilon \lesssim \frac{\Delta P_D kT}{QPeV} \frac{\frac{\pi}{2r_o} k_o}{\left[\frac{\sin k_o r_o}{k_o r_o}^3 + \frac{\sin k_o a}{k_o a^3}\right]}, \tag{5}$$

where P and T are the ambient temperature and pressure of the gas. Evaluation of the geometric factor (with the constants $r_o = 1.27$ cm, $a = 19.7$ cm, $k_o = 0.228$ cm^{-1}) and substitution of the calibration results in the expression of the charge per molecule directly in terms of the chart recorder signal yield

$$M\epsilon \lesssim \frac{\frac{\partial \Delta P_D}{\partial V_{SIG}} kT(0.45)\, V_{SIG}}{QPeV}. \tag{6}$$

Recorder plots of two runs are shown in Fig. I-10. Experimental data for these runs are the following.

P = 12 psi SF_6 (= 8.2×10^5 dyne/cm^2)

T = 300°K

Q = 1040 (Run 1), 1120 (Run 2)

V = 3500 V (rms) (= 11.7 esu).

The recorder plots show the decay of the DC coupled polarization signal used for tuning the detection circuit to below the inherent noise level, thus revealing no charge signal greater than the noise. This noise voltage is nothing but the Johnson noise in the

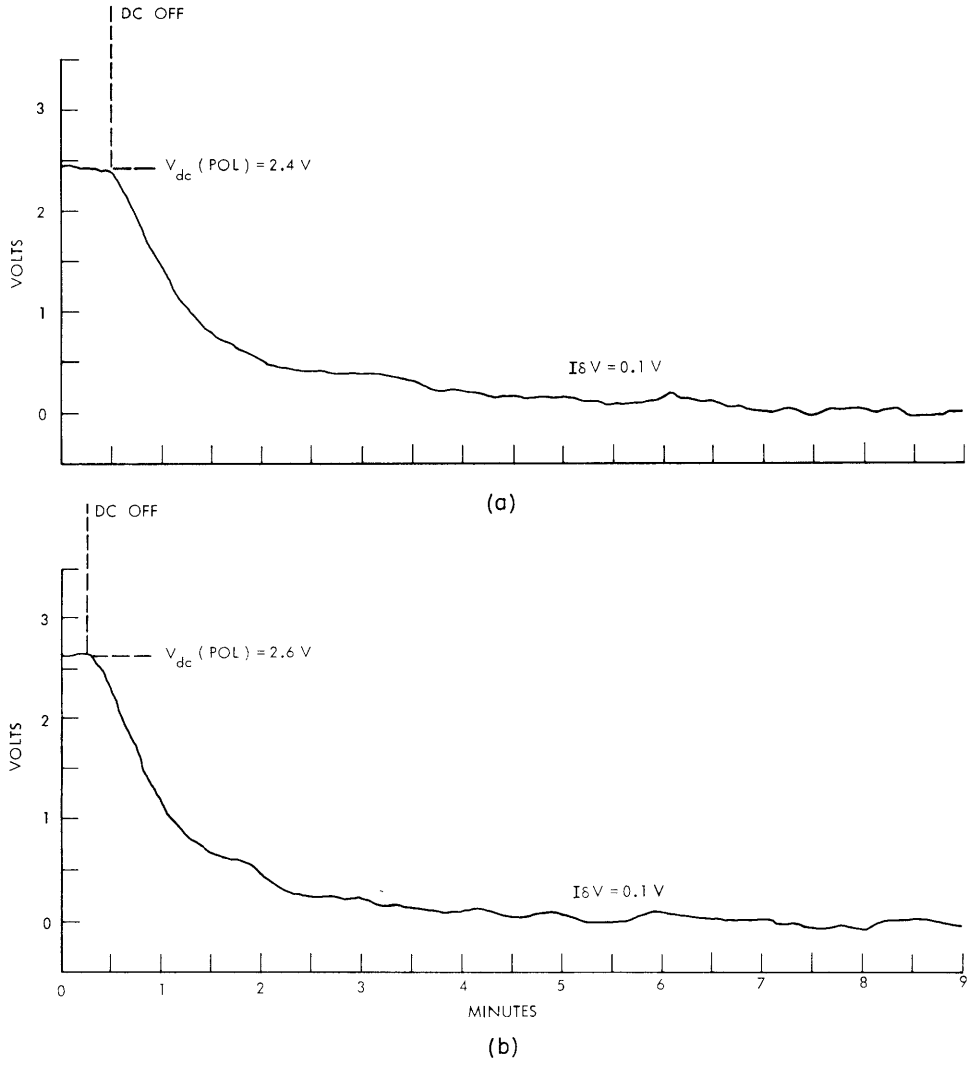

Fig. I-10. (a) Neutrality measurement: Run 1 (f = 494 Hz, Δf = 0.1 Hz).
(b) Neutrality measurement: Run 2 (f = 494 Hz, Δf = 0.1 Hz).

detection circuit, as can be seen by comparing these data with the plots of background noise shown in Fig. I-8.

If a signal attributable to a molecular charge were present, it could be seen with a signal-to-noise ratio of approximately one, if the detected signal were of 0.1 V magnitude. Substituting the value $V_{SIG} = 0.1$ V in Eq. 6 yields an upper limit for the charge on the SF_6 molecule:

$$M\epsilon \lesssim 1.9 \cdot 10^{-19}. \tag{7}$$

Dividing Eq. 7 by the mass number of SF_6 (M = 146) gives an upper limit for a fundamental electron-proton charge difference:

$$\epsilon \lesssim 1.3 \times 10^{-21}. \tag{8}$$

From Eq. 6 it is seen that the experiment gains sensitivity linearly with the electrode voltage V, and by better than a linear factor with the cavity pressure P, since the Q also increases with pressure. Both of these parameters were conservatively chosen in the initial experiment. A gain in sensitivity by a factor between 10^2 and 10^3 seems reasonably possible.

H. F. Dylla, J. G. King

References

1. R. A. Millikan, Electrons (+ and -), Protons, Photons, Neutrons and Cosmic Rays (University of Chicago Press, Chicago, Ill., 1935).
2. V. D. Hopper and T. H. Laby, Proc. Roy. Soc. (London) 178A, 243 (1941).
3. R. W. Stover, T. I. Moran, and J. W. Trischka, Phys. Rev. 164, 1599 (1967).
4. A. Picard and E. Kessler, Arch. Sci. Phys. Nat. 7, 340 (1925).
5. A. M. Hillas and T. E. Cranshaw, Nature 184, 892 (1959); 186, 459 (1960); H. Bondi and R. A. Lyttleton, 184, 974 (1959).
6. J. G. King, Phys. Rev. Letters 5, 562 (1960).
7. J. G. King, SF_6 (unpublished).
8. V. W. Hughes, Phys. Rev. 76, 474 (1949); 105, 170 (1957).
9. J. C. Zorn, G. E. Chamberlain, and V. W. Hughes, Phys. Rev. 129, 2566 (1963).
10. L. J. Fraser, E. R. Carlson, and V. W. Hughes, Bull. Am. Phys. Soc. 13, 636 (1968).
11. I. S. Shapiro and I. U. Estulin, Soviet Phys. – JETP 3, 626 (1957).
12. C. G. Shull, K. W. Billman, and F. A. Wedgwood, Phys. Rev. 153, 1415 (1967).